

The reversal of the laser-beam-induced-current contrast with varying illumination density in a $\text{Cu}_2\text{ZnSnSe}_4$ thin-film solar cell

Qiong Chen and Yong Zhang

Citation: *Appl. Phys. Lett.* **103**, 242104 (2013); doi: 10.1063/1.4844815

View online: <http://dx.doi.org/10.1063/1.4844815>

View Table of Contents: <http://apl.aip.org/resource/1/APPLAB/v103/i24>

Published by the [AIP Publishing LLC](#).

Additional information on *Appl. Phys. Lett.*

Journal Homepage: <http://apl.aip.org/>

Journal Information: http://apl.aip.org/about/about_the_journal

Top downloads: http://apl.aip.org/features/most_downloaded

Information for Authors: <http://apl.aip.org/authors>

The reversal of the laser-beam-induced-current contrast with varying illumination density in a $\text{Cu}_2\text{ZnSnSe}_4$ thin-film solar cell

Qiong Chen and Yong Zhang^{a)}

Department of Electrical and Computer Engineering, and Energy Production and Infrastructure Center (EPIC), The University of North Carolina at Charlotte, Charlotte, North Carolina 28223, USA

(Received 12 November 2013; accepted 21 November 2013; published online 10 December 2013)

We apply an array of correlated spatially-resolved techniques, including μ -Raman/photoluminescence/reflectance/laser-beam-induced-current in conjunction with scanning electron microscopy and atomic force microscopy, to study the impact of the microscopic-scale thickness inhomogeneity of CdS layer in a $\text{Cu}_2\text{ZnSnSe}_4$ thin-film solar cell. Thicker CdS regions are found to cause more light reflecting loss thus yield lower external quantum efficiencies and energy conversion efficiencies than the general area. However, these regions show much less efficiency degradation at high illumination intensity, leading to an inversion of laser-beam-induced-current contrast in the area mapping. While improving the CdS layer uniformity can boost the device performance, the finding further points out the possibility of operating thin-film photovoltaic devices based on the similar materials (such as CuInGaSe_2 , CdTe, $\text{Cu}_2\text{ZnSn(S,Se)}_4$) under a substantially higher illumination density for concentrated photovoltaic and photo-detection. © 2013 AIP Publishing LLC. [<http://dx.doi.org/10.1063/1.4844815>]

Quaternary compounds, $\text{Cu}_2\text{ZnSnS}_4$ (CZTS) and $\text{Cu}_2\text{ZnSnSe}_4$ (CZTSe), are promising absorber materials as alternative to CuInGaSe_2 (CIGS) for thin-film solar cells, because they are composed of earth-abundant and environmentally friendly elements. Since the first demonstration of a CZTSe cell in 1996,¹ a great deal of effort has been devoted in the material and device development related to $\text{Cu}_2\text{ZnSn(S,Se)}_4$ (CZT(S,Se)) based thin-film solar cells in order to explore their potential as an economically viable photovoltaic (PV) technology. CZT(S,Se) cells with >11%² and CZTSe cells with >9% efficiency³ have been reported recently.

CdS, with its relatively wide bandgap and sound chemical stability, has been widely used as a window layer in many types of thin-film solar cells such as CdTe,⁴ CIGS,⁵ and CZT(S,Se)^{2,3} devices. CdS serves at least three important functions in the device: (1) helping the formation of a p-n junction near the interface of the absorber, (2) passivating the surface states of the absorber, and (3) protecting the absorber from photo-degradation. There are numeral studies in the literature on the role of CdS in the thin-film solar device.^{6–8} The device performance is known to depend sensitively on the CdS layer thickness. However, the previous attention was focused on the optimization over the (average) layer thickness. In this work, we investigate the impact of the microscopic-scale thickness inhomogeneity of CdS on the CZTSe device, using μ -Raman/photoluminescence (PL)/laser-beam-induced-current (LBIC)/reflectance, with sub-micron spatial resolution, and correlating with scanning electron microscopy (SEM)/atomic force microscopy (AFM). The results suggest how to determine the appropriate CdS layer thickness for the thin-film PV device potentially operating under different illumination densities and offer

more insights to the roles that CdS and other possible “window” layers may play in the related PV devices.

The device used in this study is similar to those reported in Ref. 3. The CZTSe cell (M3599_23) was measured under air mass (AM) 1.5 with these results: energy conversion efficiency $\eta = 8.07\%$, short-circuit current $I_{\text{sh}} = 15.0 \text{ mA/cm}^2$, open-circuit voltage $V_{\text{oc}} = 0.344 \text{ V}$, and fill factor $\text{FF} = 65.8\%$. The device was fabricated on a soda-lime glass substrate, with $1 \mu\text{m}$ sputtered Mo back contact and 150 \AA e-beam evaporated NaF precursor. The CZTSe film was grown by a vacuum co-evaporation method with a thickness about $1 \mu\text{m}$. Device was finished with chemical bath deposited CdS, a sputtered resistive/conductive ZnO bi-layer, electron-beam-evaporated Ni/Al grids, an MgF_2 antireflective coating, and photolithographic device isolation. Details for the film growth and device processing can be found in Refs. 3 and 9.

μ -Raman/PL/reflectance measurements were performed with a Horiba Jobin Yvon HR800 confocal Raman system with a CCD detector using a 532 nm laser. With a $100\times$ (numerical aperture (NA)=0.9) objective lens, the diffraction limit laser spot size is $\sim 0.72 \mu\text{m}$, and the spatial resolution is about half of the spot size. To prevent heating effect or (irreversible) material damage, the laser power was kept below 0.2 mW, or the power density smaller than $5 \times 10^4 \text{ W/cm}^2$. μ -LBIC measurements were performed using the same system, with two gold plated probes, both 532 nm and 633 nm lasers, and in both DC and AC modes. In the DC mode, the I-V curves were measured by Keithley 2401 Source Meter Unit. In the AC mode, the laser was modulated with a mechanical chopper at 100 Hz, and the photocurrent was measured using a SR830 lock-in amplifier with a SR570 low noise current pre-amplifier. The LBIC mapping was performed in the AC mode and the LBIC data were converted into external quantum efficiencies (EQEs) by using a Si reference cell (PV Measurements, Inc.), which is verified by

^{a)} Author to whom correspondence should be addressed. Electronic mail: yong.zhang@uncc.edu

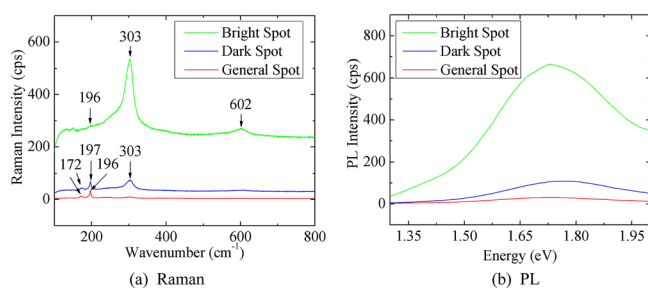


FIG. 1. Raman and PL spectra from three types of regions.

directly computing $(I/e)/(P/h\nu)$ with less than 3% discrepancy, where I is the measured photo current and P is the laser power. The reflectance was obtained with the help of an Al mirror with its reflectance curve provided by the vendor. All the measurements were performed at room temperature.

On a microscopic scale, a typical CZTSe device has been found to exhibit some degree of spatial inhomogeneity due to the thickness fluctuation of CdS layer. Three distinctly different types of regions (referred to as general area, dark spot, and bright spot) can be observed on a finished CZTSe device under optical microscope with white light illumination. Figure 1 shows the comparison of typical Raman and PL spectra from the three regions, measured with the 532 nm laser. In Fig. 1(a), the Raman spectrum of the general area shows the two Raman modes typically observed in CZTSe: 172 and 196 cm^{-1} ,¹⁰ with an additional weak peak at 303 cm^{-1} . This 303 cm^{-1} peak is found to be strongly enhanced at both dark and bright spots, in particular, with the appearance of another peak of 602 cm^{-1} at the bright spot. These two peaks match, respectively, the longitudinal optical (LO) and 2LO Raman modes of CdS. The observed enhancement can be understood as the resonant Raman effect of CdS,¹¹ since the excitation energy of the 532 nm laser (~ 2.33 eV) is rather close to that of the CdS bandgap (2.42 eV) and the similar resonant effect has been reported previously in polycrystalline CdS thin films.¹² In addition, as shown in Fig. 1(b), both bright and dark spots give rise to a

broad PL band at 1.73 eV, which is far above the bandgap of CZTSe (~ 0.96 eV),³ presumably associated with defects in the polycrystalline CdS.¹³ Neither the 303 and 602 cm^{-1} nor the 1.73 eV spectral features were observed on the nominally same material but without the layers beyond CZTSe. Therefore, it is reasonable to assume that the CdS layer is the thickest at the bright spot and thinnest at the general area, which was confirmed by SEM and AFM measurements to be presented later. The unintended CdS layer thickness fluctuation provides an opportunity for us to examine the effect of the microscopic scale fluctuation of the CdS layer thickness on the device performance with minimal variations over many other possible growth parameters and device processing conditions. This goal is accomplished in this work by performing an array of mutually correlated microscopic characterizations from the same area of the device.

Figure 2 collects the 2D imaging or mapping data of optical microscope, SEM, reflectance, Raman, PL, and LBIC, all acquired approximately from a single $20\ \mu\text{m} \times 20\ \mu\text{m}$ area on the device with the $100\times$ objective lens. Fig. 2(c) (reflectance) was obtained with ~ 18 pW ($\sim 4.4 \times 10^{-3}$ W/cm^2), Fig. 2(f) (LBIC) with $\sim 2\ \mu\text{W}$ power ($\sim 4.9 \times 10^2$ W/cm^2), and Figs. 2(d) (Raman) and 2(e) (PL) with $200\ \mu\text{W}$ power ($\sim 4.9 \times 10^4$ W/cm^2), all with the 532 nm laser. The optical image (Fig. 2(a)) reveals a bright region of a few μm size near the center and some scattered dark spots, corresponding to the CdS rich regions mentioned above. The SEM image (Fig. 2(b)) confirms the variations in surface morphology. The extra height of the bright region is estimated to vary from 1 to 1.5 μm using AFM. The reflectance mapping result (Fig. 2(c)) is in general agreement with the optical image, because both resulting from reflection. It indicates that the large CdS rich region is much more reflective, with maximum reflectivity $\sim 21\%$, than the general area. However, the smaller CdS rich regions appear to be less reflective than the general area. The minimum reflectivity is $\sim 1.5\%$. The Raman (Fig. 2(d), monitored at 303 cm^{-1}) and PL (Fig. 2(e), monitored at 1.73 eV) mapping data reveal clearly stronger signals from the bright region, as shown in

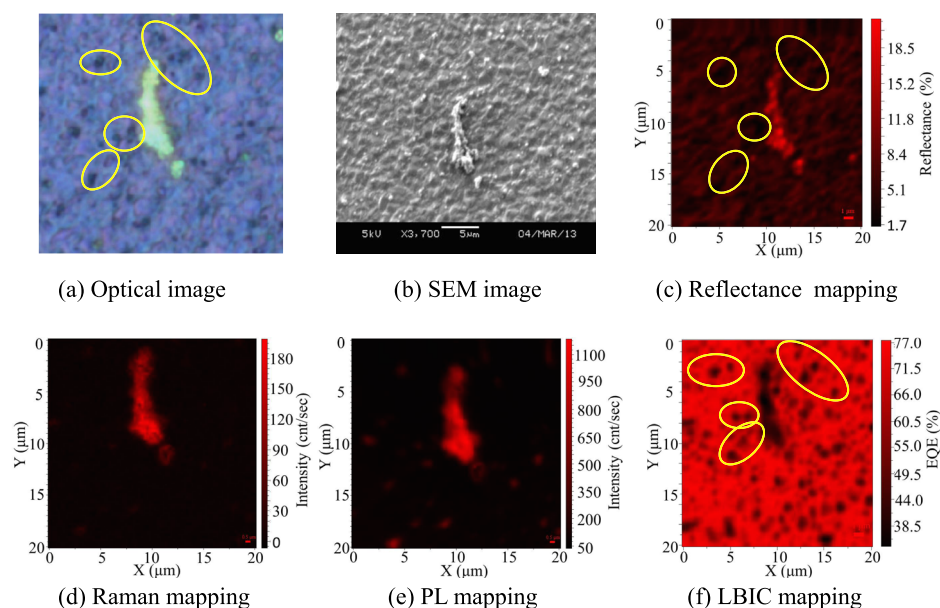


FIG. 2. 2D imaging and mapping results of a CZTSe cell.

Fig. 1. As expected and indeed observed, in Fig. 2(f), the CdS rich regions (the large island and dark spots in the optical image) yield much smaller photocurrents, reduced by as much as a factor of 2 or more, than the general area. A few dark spots are circled in both Figs. 2(a) and 2(f) to show the correlation. Furthermore, there is a generally anti-correlation between the reflectance and LBIC data (Figs. 2(c) and 2(f)). These findings suggest that improving the thickness uniformity of CdS will improve the average short-circuit current of the device at least to some extent.

More interesting findings come from the laser power dependence of the LBIC mapping data. In Fig. 3 (at 532 nm) and Fig. 4 (at 633 nm), we compare the reflectance mapping with the LBIC mapping of the same area under two representative low and high laser powers. The corresponding histogram plots are also given with the LBIC data being converted into EQEs. By “low power,” we mean the power level that can yield an average EQE comparable to the macroscopic probe, whereas by “high power” the EQE of the general area shows significant degradation, but the power is not as high as to cause permanent damage to the material. Note that the macroscopic specular reflectance from the device surface is rather small, $\sim 0.85\%$ at 532 nm and 1.2% at 633 nm, because the rough sample surface leads to significant diffuse reflectance or scattering. With the use of high NA objective lens, we were able to capture a major portion of the scattered light, yielding much higher “reflectance,” for instance, 5.1% in average (not including the large CdS island) at 532 nm. For the LBIC mapping data, at the low

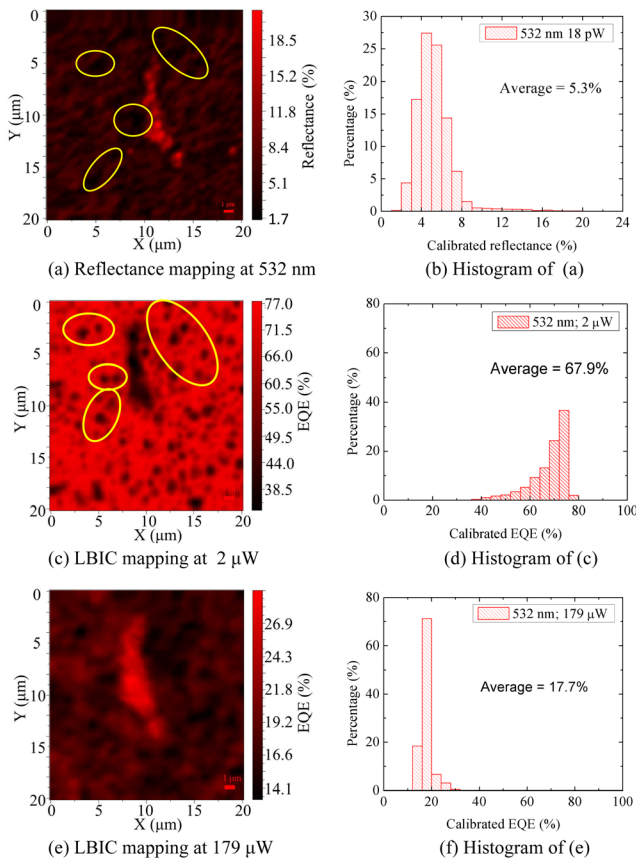


FIG. 3. Reflectance and LBIC mapping with 532 nm laser at low and high power levels.

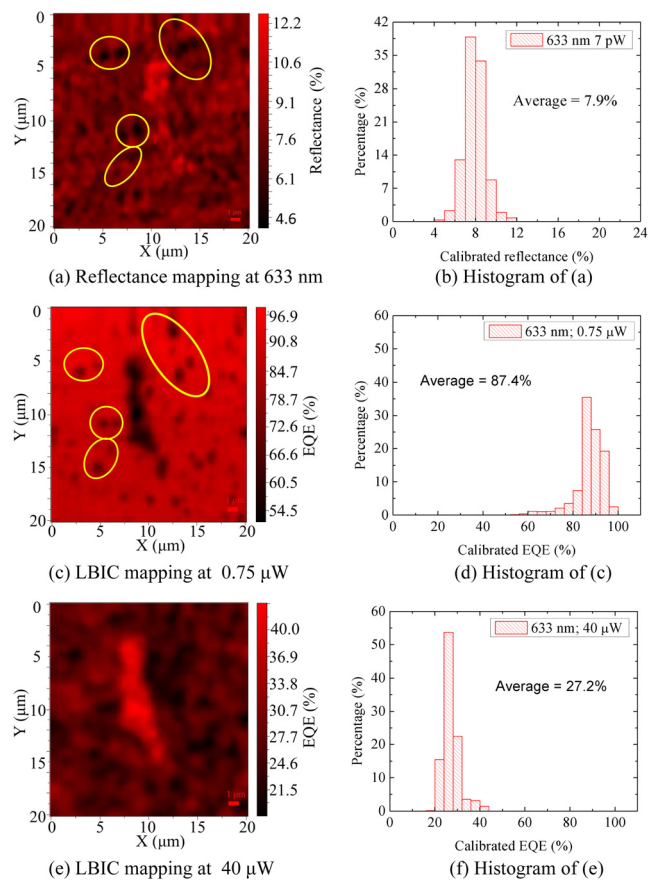


FIG. 4. Reflectance and LBIC mapping with 633 nm laser at low and high power levels.

power level, for both wavelengths, the device shows rather high average EQE (averaged over the mapped area): $67.9 \pm 0.3\%$, varying from 34.3% to 77.6% for $2 \mu\text{W}$ – 532 nm (Fig. 3(c)), and $87.4 \pm 1.3\%$, varying from 52.1% to 98.6% for $0.75 \mu\text{W}$ – 633 nm (Fig. 4(c)). The average values are consistent with the macroscopic data of a similar device: $\sim 81\%$ at 532 nm and $\sim 90\%$ at 633 nm . However, at the high power level, the average EQEs reduce drastically down to $17.7\% \pm 2.3\%$ at $167 \mu\text{W}$ – 532 nm (Fig. 3(e)) and $27.2\% \pm 1.1\%$ at $40 \mu\text{W}$ – 633 nm (Fig. 4(e)). Interestingly, the reductions at the bright spot are much smaller: from $\sim 45\%$ ($2 \mu\text{W}$) to $\sim 25\%$ ($167 \mu\text{W}$) for 532 nm ; from $\sim 65\%$ ($0.75 \mu\text{W}$) to $\sim 40\%$ ($40 \mu\text{W}$) for 633 nm , which leads to the reversal of the LBIC contrast, as evident between Figs. 3(c) and 3(e) or Figs. 4(c) and 4(e). Clearly, the device region with a thicker CdS layer is more immune to the EQE droop with increasing illumination power, although the thicker region has a lower initial EQE. One possible mechanism could be that the electronic structure of the CZTSe/CdS heterojunction, such as the effective barrier height, depends sensitively on the CdS layer thickness. The low initial EQE of the CdS rich region is likely related to the properties of CdS: the high reflectivity and residual absorption near the bandgap, the poor carrier transport of the polycrystalline phase. These issues could, in principle, be mitigated or improved to allow the adoption of thicker CdS layer, in particular for high illumination applications either in concentrated PV or photo-detection. Comparing Figs. 3 and 4, one can also find that the thicker CdS layer affects the device

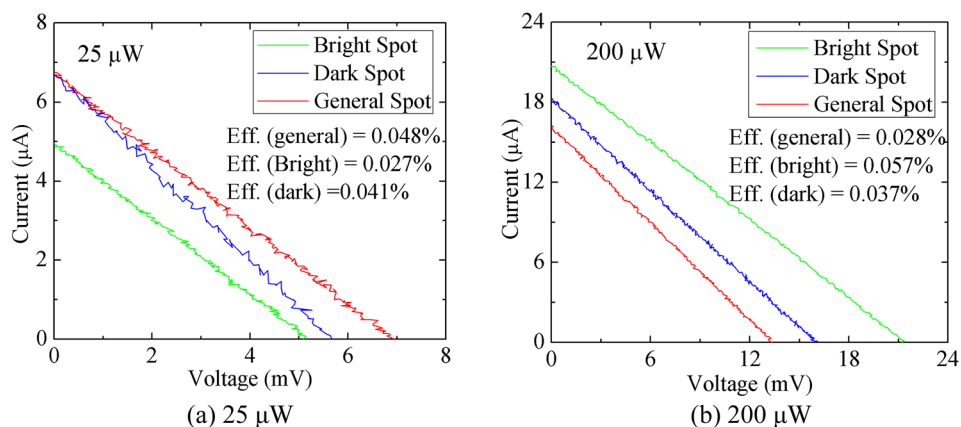


FIG. 5. I-V curves of three types of regions with 532 nm laser at low and high power levels.

performance more at 532 nm than 633 nm. In the reflectance mapping, the bright spot reflects four times as much light as the general area with 532 nm, but with 633 nm, the difference is smaller. Under both low and high power levels, the LBIC contrast with 532 nm is also stronger than with 633 nm.

We further studied the I-V characteristic of the device with varying laser power. Figure 5 compares I-V curve of three different regions at 25 μW and 200 μW with 532 nm laser. At 25 μW, the general area yields the largest values in both I_{sc} and V_{oc} . However, at 200 μW, the bright spot exceeds the general area by 29% in I_{sc} , which is consistent with LBIC mapping data at different laser levels, and 60% in V_{oc} . The local energy conversion efficiency of CdS rich region has increased from 0.027% at 25 μW to 0.057% at 200 μW. On the other hand, the efficiency of the general region has decreased by almost a factor of two with increased laser power. Note that the observed low values in the absolute efficiency are largely due to the fact that the V_{oc} and FF values are substantially lower in the microscopic probe than those under large area illumination, although I_{sc} values are similar to those measured under the large area illumination. The low V_{oc} under the tightly focused local excitation is because the external bias is applied across the whole device area of which the most is dark, and thus the locally generated photocurrent is mostly cancelled by the forward current passing through the non-illuminated area in the opposite direction. Therefore, the efficiencies derived above are not the actual efficiencies of the local region under illumination, but only used to serve as qualitative measures of the changes. The finding suggests that one might be able to optimize the CdS layer thickness for the device to operate at a higher illumination density, potentially much above that of AM1.5.

Three distinctly different types of regions, bright, dark, and general area, in the order of decreasing CdS layer thickness, were found on a CZTSe device surface and investigated using spatially resolved techniques, including μ -Raman/PL/reflectance/LBIC, SEM, and AFM. The bright spot, which is mostly CdS rich, showed strong LO and 2LO CdS resonant Raman lines at 303 and 602 cm^{-1} , and a strong PL band at 1.73 eV related to defects in the polycrystalline CdS. The regions with thicker CdS layer were found to be substantially

more or less reflective, depending on the thickness. However, the thicker CdS layer is much more immune than the general area to the efficiency droop, thus leading to the reversal of the LBIC contrast with increasing illumination intensity. These findings on one hand point to the possibility of increasing the cell efficiency by improving the microscopic uniformity of the CdS window layer, and on the other hand, perhaps more significant and interesting, suggest the potential to fabricate CZTSe and related thin-film solar cells or photo-diodes for concentrated PV and photo-detection.

We are very grateful to Dr. I. Repins for providing the samples and discussions, Dr. Da Li and Dr. Naili Yue for assistance in measurements, and Dr. S. Choi for helpful discussions on Raman data. Y.Z. acknowledges the support of Bissell Distinguished Professorship.

- ¹H. Katagiri, N. Sasaguchi, S. Hando, S. Hoshino, J. Ohashi, and T. Yokota, *Sol. Energy Mater. Sol. Cells* **49**, 407 (1997).
- ²T. K. Todorov, J. Tang, S. Bag, O. Gunawan, T. Gokmen, Y. Zhu, and D. B. Mitzi, *Adv. Energy Mater.* **3**, 34 (2013).
- ³I. Repins, C. Beall, N. Vora, C. Dehart, D. Kuciauskas, P. Dippo, B. To, J. Mann, W. Hsu, A. Goodrich, and R. Noufi, *Sol. Energy Mater. Sol. Cells* **101**, 154 (2012).
- ⁴X. Wu, *Solar Energy* **77**, 803 (2004).
- ⁵I. Repins, M. Contreras, B. Egaas, C. DeHart, J. Scharf, C. Perkins, B. To, and R. Noufi, *Prog. Photovoltaics* **16**, 235 (2008).
- ⁶K. Nakamura, M. Gotoh, T. Fujihara, T. Toyama, and H. Okamoto, *Solar Energy Mater. Sol. Cells* **75**, 185 (2003).
- ⁷B. Korevaar, A. Halverson, J. Cao, J. Choi, C. Collazo-Davila, and W. Huber, *Thin Solid Films* **535**, 229 (2013).
- ⁸K. Orgassa, U. Rau, Q. Nguyen, H. Schock, and J. Werner, *Prog. Photovolt: Res. Appl.* **10**, 457 (2002).
- ⁹N. Vora, J. Blackburn, I. Repins, C. Beall, B. To, J. Pankow, G. Teeter, M. Young, and R. Noufi, *J. Vac. Sci. Technol. A* **30**, 051201 (2012).
- ¹⁰M. Grossberg, J. Krustok, J. Raudoja, K. Timmo, M. Altosaar, and T. Raadik, *Thin Solid Films* **519**, 7403 (2011).
- ¹¹R. C. C. Leite, J. F. Scott, and T. C. Damen, *Phys. Rev. Lett.* **22**, 780 (1969).
- ¹²X. Wu, R. G. Dhere, Y. Yan, M. J. Romero, Y. Zhang, J. Zhou, C. DeHart, A. Duda, C. Perkins, and B. To, in *Proceedings of the 29th IEEE PVSC Photovoltaic Specialists Conference*, New Orleans, Louisiana, USA, 20–24 May 2012, p. 531.
- ¹³A. E. Abken, D. P. Halliday, and K. Durose, *J. Appl. Phys.* **105**, 064515 (2009).